Assessment of Mouse-Specific Pharmacokinetics in Kidneys Based on 131I Activity Measurements Using Micro-SPECT

Clarita Saldarriaga Vargas (csvargas@sckcen.be)
Belgian Nuclear Research Centre (SCK CEN) https://orcid.org/0000-0002-1156-8713
Lara Struelens
Belgian Nuclear Research Centre (SCK CEN)
Matthias D'Huyvetter
Vrije Universiteit Brussel
Vicky Caveliers
Vrije Universiteit Brussel
Peter Covens
Vrije Universiteit Brussel

Original research

Keywords: micro-SPECT, activity quantification, accuracy, kidney, mouse-specific pharmacokinetics

Posted Date: July 1st, 2021

DOI: https://doi.org/10.21203/rs.3.rs-660534/v1

Abstract

Background

In order to acquire accurate drug pharmacokinetic information, such as that required for tissue dosimetry, micro-SPECT must be quantitative and allow an accurate assessment of radioligand activity in the relevant tissue. This study investigates the feasibility of deriving accurate mouse-specific time-integrated drug pharmacokinetic data in mouse kidneys from activity measurements using micro-SPECT.

Methods

An animal experiment was done to evaluate the accuracy of ^{131}I activity quantification in mouse kidneys using a micro-SPECT system against conventional *ex vivo* gamma counting (GC) in a NaI(Tl) detector. The imaging setting investigated was that of the mouse biodistribution of a ^{131}I-labelled single-domain antibody fragment (sdAb) currently being investigated for targeted radionuclide therapy of HER2-expressing cancer. SPECT imaging of ^{131}I 365-keV photons was done with a VECTor/CT system (MILabs, Netherlands) using a high-energy mouse collimator with 1.6-mm-diameter pinholes. For each activity quantification technique, the pharmacokinetic profile from approximately 1 to 73 h p.i. of the radioligand was derived and the time-integrated activity coefficient per gram of tissue ($\tilde{a}/M$) was estimated. Additionally, SPECT activity recovery coefficients were determined in a phantom setting.

Results

SPECT activities underestimate the reference activities by an amount that is dependent on the ^{131}I activity concentration in the kidney, and thus on the time point of the pharmacokinetic profile. This underestimation is around − 12% at 1.5 h (2.78 MBq.mL^{-1} mean reference activity concentration), -13% at 6.6 h (143 kBq.mL^{-1}), -40% at 24 h (15 kBq.mL^{-1}) and − 46% at 73 h (5 kBq.mL^{-1}) p.i. The $\tilde{a}/M$ value estimated from SPECT activities is, nevertheless, within − 15% from the reference (GC) $\tilde{a}/M$ value. Furthermore, better quantitative accuracy (within 2% from GC) in the SPECT $\tilde{a}/M$ value is achieved when SPECT activities are compensated for partial recovery with a phantom-based correction factor.

Conclusion

The SPECT imaging system used, together with a robust activity quantification methodology, allows an accurate estimation of time-integrated pharmacokinetic information of the ^{131}I-labelled sdAb in mouse kidneys. This opens the possibility to perform mouse-specific kidney-tissue dosimetry based on pharmacokinetic data acquired *in vivo* on the same mice used in nephrotoxicity studies.

1 Introduction

Pharmacokinetic data derived from preclinical studies in *in vivo* biological models play a key role in the prediction of radiation dosimetry of first-in-human studies of targeted radionuclide therapy. Accurate quantification of

radioligand activity in preclinical radiobiological studies is necessary for a sound investigation of the preclinical absorbed dose to normal (healthy) animal tissues.

Targeted radionuclide therapy with radioligands based on small targeting molecules, such as peptides and antibody fragments, which typically show a significant retention in kidney tissue, can pose a concern in terms of radiation-induced nephrotoxicity. Consequently, the kidneys are often the subject of pharmacokinetic and dose-escalation studies during the preclinical testing of (new) radioligands.

Over the past two decades small-animal single-photon computed tomography (micro-SPECT) has seen significant improvements in spatial and temporal resolution, sensitivity and quantitative capability, leading to a growing use of this technique for quantitative imaging studies of drug pharmacokinetics in basic and (back)translational research [1, 2, 3]. As opposed to conventional radioactivity measurements of dissected (*ex vivo*) tissues via gamma counting (GC), which requires animal sacrifice and the use of multiple animals for sampling at different time points to obtain drug pharmacokinetics, micro-SPECT offers the possibility to quantify radioactivity in tissues *in vivo*, allowing to derive pharmacokinetic information from one and the same animal. This, not only eliminates the inter-variability effects in the assessment of the time dependence of drug pharmacokinetics, since each animal acts as its own control for different sampling time points, but also enables the possibility to perform mouse-specific dosimetry on animals used in (long-term) radiobiological studies of therapeutic response and toxicity.

In order to obtain accurate drug pharmacokinetic information, micro-SPECT must be quantitative and allow an accurate assessment of radioactivity in the relevant tissue. Similar to clinical SPECT, however, the accuracy of micro-SPECT images can be influenced by several factors. These include scatter and non-uniform attenuation of photons in tissue [4], partial volume effects (PVE) due to the limited spatial resolution of the imaging system [4], statistical and bias effects associated with the image reconstruction methods in relation with some imaging conditions (e.g. low-count studies, poor signal-to-noise ratio) [5, 6], artefacts resulting from the use of resolution modelling [7], etc. [8]. While methods to compensate for photon Compton scatter and attenuation are available and have been adopted in micro-SPECT [9, 10], the other effects strongly depend on the specific activity set-up and the imaging and reconstruction settings used, and are still difficult to accurately compensate directly and generally (i.e. for any imaging setting) on SPECT images. Yet, an approach to compensate for bias in SPECT activity recovery (such as that resulting from PVE and image reconstruction effects) post-reconstruction consists of applying a correction factor based on activity recovery coefficients (ARC) determined for specific (phantom) imaging conditions. Although this approach is more and more used in clinical theranostics relying on quantitative SPECT [11], currently it is usually not considered in preclinical quantitative micro-SPECT studies. Last but not least, in addition to SPECT technique-related factors, the accuracy of activity quantification based on SPECT can also be affected by the methods used for image quantification (e.g. delineation of VOI), activity calibration (accuracy and reproducibility of procedures), image processing post-reconstruction (e.g. use of image denoising filters), etc.; so these aspects should also be considered carefully in the design and reporting of small-animal quantitative SPECT studies [12, 13].

This study evaluates the accuracy of Iodine-131 (^{131}I) activity quantification in mouse kidneys using a micro-SPECT/CT imaging system and investigates the feasibility of this approach to derive mouse-specific time-integrated pharmacokinetic information as input for radiation dosimetry. The imaging setting investigated was that of the mouse biodistribution of the single-domain antibody fragment (sdAb) 2Rs15d radiolabelled with ^{131}I, a radioligand previously reported and described in [14] which is currently being tested in humans for targeted radionuclide therapy of HER2-expressing cancer [15]. Considering the relevant retention of this sdAb in kidneys, an

investigation on the accuracy of micro-SPECT imaging for assessing pharmacokinetics in mouse kidneys is pertinent to support (back)translational investigations on the dose-response of potential nephrotoxicity and radioprotective strategies. Additionally, a phantom study is performed to investigate the influence on SPECT activity recovery of the number of photon counts used for image reconstruction, as well as the use of phantom-based recovery coefficients for improving the accuracy of micro-SPECT-based activity quantification.

2 Materials And Methods

The radioligand used in this study was the [^{131}I]SGMIB-labelled anti-HER2 sdAb 2Rs15d, previously reported elsewhere [14]. All reagents were purchased from Sigma-Aldrich (Darmstadt, Germany) unless otherwise stated. Sodium [^{131}I]iodide was purchased from Perkin-Elmer.

Anti-HER2 sdAb 2Rs15d was generated as described previously [16]. 2Rs15d sdAb was radiolabelled with ^{131}I via the residualizing prosthetic group N-Succinimidyl 4-guanodinomethyl-3-[^{131}I]iodobenzoate ([^{131}I]SGMIB) and purified as reported previously [14].

All animal experiments were done using healthy female C57BL/6 mice (8–10-week old, 19.4 ± 1.3 g body weight mean ± standard deviation (SD)) and were conducted according to the guidelines and after approval of the Ethical Committee of the Vrije Universiteit Brussel.

2.1 Evaluation of accuracy of SPECT-based activity quantification

An animal experiment was done to evaluate the accuracy of SPECT-based activity quantification of ^{131}I in mouse kidneys against conventional *ex vivo* activity measurements in a gamma counter. Mice were anesthetised by inhalation with 2% isoflurane and were intravenously injected in the tail vein with 11.5 ± 1.8 MBq [^{131}I]-sdAb (5 µg sdAb). A total of 14 mice, divided in four groups (one group per time point), were imaged with SPECT/CT at around 1.5 (n = 3 mice), 6.6 (n = 3), 24 (n = 5) and 73 (n = 3) h post injection (p.i.) of the radioligand (Table 1). For the first two time points (time points during fast pharmacokinetics), mice were first euthanized by cervical dislocation, and SPECT-CT scans were done immediately *ex vivo* on their carcasses, after which both kidneys were dissected. Mice imaged at around 24 and 73 h p.i. (time points during slower pharmacokinetics) however, were imaged *in vivo*, euthanized and dissected immediately after SPECT-CT imaging. The kidneys of all mice were weighted, and their activity was assessed in the gamma counter. Radioactivity in kidney was corrected for the physical decay between the reference time (t_{ref}) of the activity measurement with each technique (start of GC measurement, and start and middle time of the scan for respectively *ex vivo* and *in vivo* SPECT) and the mouse time of death.

For each mouse kidney, the percentage deviation of the activity determined with SPECT (A_{SPECT}) from the reference activity determined with gamma counting (A_{GC}) was calculated. The mean deviation of kidneys (both left and right) of all mice per time point was calculated. Two-tailed paired t-tests were applied to the datasets of each time point to determine the significance of differences between SPECT and GC activity data. Statistical significance was defined as $p < 0.05$.

Additionally, for each mouse kidney the fraction of injected activity per gram of dissected tissue (*FIA/g*) was calculated. For each activity quantification technique, the pharmacokinetic profile was derived from the kidney *FIA/g* of all mice (n = 14) as a function of time p.i. (hereafter referred to as datasets GC1 for gamma counting data,

and SS1 for single SPECT data), and the time-integrated activity coefficient ($\tilde{a}$) per gram of tissue (M) was estimated (cfr. calculation details in Sect. 2.4).

Using the time-dependent fit function derived from pharmacokinetic dataset GC1, the kidney *FIA/g* was estimated at the time point halfway between the start and the end of *in vivo* SPECT scans, and at the mouse time of death, and the deviation between the resulting *FIA/g* values was calculated. This was used to estimate the potential bias (over-response) associated with SPECT measurements performed *in vivo* when compared with GC measurements, due to the estimated (expected) decrease in radioligand uptake in the kidneys during the (scan) time prior to death.

Table 1

Acquisition settings of single SPECT scans performed on 14 mice injected with the [^{131}I]-labelled sdAb (dataset SS1), used for the comparison of kidney activity against gamma counting.

Av. time p.i. to death [max. range of variation between mice] (h)	Animal setting	No of mice, *n*	No of bed positions	Scan time per bed position (s)	Total effective scan time (min)	Av. (of *n* mice) of total scan counts acquired in photo peak window	Av. (of *n* mice) of photo peak counts used as background and scatter
1.5 [± 0.0]	*ex vivo*	3	20	66	22	4.5E + 06	5.0E + 05
6.6 [± 0.0]	*ex vivo*	3	20	66	22	8.1E + 05	1.7E + 05
24.3* [± 0.8]	*in vivo*	5	20	225	75	1.0E + 06	4.5E + 05
73.4** [± 2.0]	*in vivo*	3	20	239	80	8.6E + 05	4.4E + 05
* 23.6 h average time p.i. to middle of scan.							
** 72.6 h average time p.i. to middle of scan.							

2.2 Pharmacokinetic assessment *ex vivo* using gamma counting

As part of the previous animal experiment, kidney uptake (in *FIA/g*) was assessed additionally at 3.2 and 48 h p.i. of the radioligand, but kidney activity was determined only via GC measurements. These mice (n = 3 per time point) were injected with 4.35 ± 0.09 MBq [^{131}I]-sdAb. The time-integrated pharmacokinetic parameter $\tilde{a}/M$ was estimated (cfr. calculation details in Sect. 2.4) from all the kidney *FIA/g* determined with GC in this (3.2 and 48 h p.i.) and the previous section (1.5, 6.6, 24 and 73 h p.i) (hereafter referred to as dataset GC1ext), to set a reference for comparison for the $\tilde{a}/M$ values determined from longitudinal SPECT scans (cfr. section 2.3).

2.3 Pharmacokinetic assessment using longitudinal SPECT imaging

A longitudinal quantitative SPECT/CT imaging study was performed on 5 mice to evaluate the feasibility of deriving mouse-specific pharmacokinetic information of the [^{131}I]-sdAbs. All mice were intravenously injected with 13.62 ± 1.15 MBq [^{131}I]-sdAb. Sequential SPECT-CT scans were performed *in vivo* on each mouse, starting at approximately 1, 3, 6, 24, 46 and 70 h p.i. of the radioligand (cfr. acquisition settings in Table 2). Immediately after the last scan, mice were euthanized and both kidneys were dissected and weighted. Kidney activities were determined from SPECT images (cfr. section 2.5) using as a reference time the middle time of each SPECT scan. The *FIA/g* was calculated at each scan time point, and the time-integrated pharmacokinetic parameter $\tilde{a}/M$ was

estimated (cfr. calculation details in Sect. 2.4) from the pharmacokinetic profile of each mouse (hereafter referred to as datasets LS1, LS2, LS3, LS4 and LS5, i.e. one dataset per mouse).

Table 2

Acquisition settings of the longitudinal SPECT scans performed *in vivo* on 5 mice injected with the [^{131}I]-labelled sdAb, corresponding to datasets LS1-LS5.

Av. scan start time p.i. [max. range of variation between mice] (h)	No of bed positions	Scan time per bed position (s)	Total effective scan time (min)	Av. (of *n* mice) of total scan counts acquired in photo peak window	Av. (of *n* mice) of photo peak counts used as background and scatter
1.0 [± 0.0]	20	51	17	4.9E + 06	5.2E + 06
3.3 [± 0.0]	20	66	22	1.7E + 06	2.4E + 06
6.0 [± 0.1]	20	66	22	1.1E + 06	2.0E + 05
24.2 [± 2.0]	20	150	50	8.2E + 05	3.0E + 05
46.3 [± 3.7]	20	239 (159)*	80 (53)*	9.1E + 05 (6.0E + 05)*	4.4E + 05 (3.1E + 05)*
70.2 [± 3.3]	20	239 (159)*	80 (53)*	7.8E + 05 (5.2E + 05)*	4.0E + 05 (2.8E + 05)*
* specification used for the two mice from datasets LS1 and LS2.					

2.4 Pharmacokinetic modelling

Kidney pharmacokinetic data were analysed by nonlinear least squares fitting (MATLAB R2019a, MathWorks, Massachusetts, USA) to a mathematical function of time elapsed p.i. (t). A negative power function with two coefficients (c_1 and c_2) (Eq. 1) was chosen among the various mathematical functions considered (cfr. supplementary data). Eight datasets of *FIA/g* as a function of time (datasets GC1, SS1, GC1ext and LS1-LS5) were analysed. The Pearson's correlation coefficient (R^2) was used to quantify goodness of fit.

$$FIA(t)/g \cong c_1\, t^{-c_2} \qquad Eq.\ 1$$

The time-integrated pharmacokinetic parameter *ã/M* was calculated for the left kidneys from mathematical integration of the fit function from 1.5 h to 72 h only, since the purpose of estimating *ã/M* was only to compare different datasets and this was the common period p.i. covered by most datasets.

2.5 SPECT-CT imaging and image quantification

SPECT-CT acquisitions were performed with a VECTor/CT small-animal SPECT-CT system (U-PET/SPECT4, CT Skyscan1178; MILabs, Utrecht, Netherlands) [17]. For photon detection the SPECT module uses three stationary large NaI(Tl) detectors each with a thickness of 18 mm. A high-energy mouse collimator with 114 pinholes of 1.6-mm diameter was used for imaging of 365-keV photons of ^{131}I. A scan field-of-view with a 20-mm axial length located on the abdominal region comprising the kidneys was used for all mouse SPECT scans. Additional SPECT acquisition settings are reported in Tables 1 and 2. Following a SPECT scan, a whole-body CT scan (55 kV X-ray tube voltage, 615 µA tube current) was acquired.

SPECT and CT images were generated and co-registered with VECTor's manufacturer-provided software. SPECT images with 0.6-mm-wide cubic voxels were reconstructed using a 20% photo-peak window centred at 365 keV, using VECTor's pixel-based ordered-subset expectation maximization (OSEM) iterative reconstruction algorithm [18]. Thirty iterations with two subsets (i.e. 60 OSEM updates, equivalent to 60 maximum-likelihood expectation-maximization iterations) were performed for all scans. A prior investigation indicated that 60 OSEM updates were sufficient to ensure convergence in the recovery of hot rods with a diameter in the range of 4 to 6 mm, which we consider to be comparable to the size of mouse kidneys. A system response matrix optimized for 364 keV photons was used [19]. Two adjacent background-and-scatter windows of approximately 6% width were used for Compton photon scatter and background signal correction using the triple-energy-window method [9]. Additionally, SPECT images were registered to CT images and the resulting SPECT images were corrected for photon attenuation based on CT data [10]. No post-reconstruction filters (for smoothing) were used. The final resampled SPECT images used for analysis have nearly cubic voxels of approximately 0.17-mm width.

SPECT voxel data (count rate, in reconstructed "cps") were calibrated in terms of activity concentration ($MBq.mL^{-1}$) using a calibration factor determined from the SPECT scan of a syringe containing a [^{131}I]-NaI solution with a calibrated activity concentration directly traceable to high-resolution gamma spectrometry (more details in the supplementary data).

Image quantification was done with AMIDE 1.0.4 [20]. The amount of ^{131}I activity in the kidneys was determined from activity-calibrated SPECT images using ellipsoidal VOI. A VOI was manually drawn over each kidney based on the CT image, and its position and proportions were then fine-tuned visually according to the SPECT image. The VOI volume was adjusted to match the kidney volume estimated from the mass of the dissected kidney and an assumed tissue density of $1.04\ g.mL^{-1}$.

2.6 Gamma counting, GC

The activity of dissected tissues was measured in a Cobra II model 5003 gamma counter (Canberra-Packard, Schwadorf, Austria) using a measurement protocol optimized to limit the overall measurement uncertainty (cfr. details in the supplementary data).

The activity calibration of GC measurements was directly traceable to high-resolution gamma spectrometry (cfr. section 2.7). The calibration procedure of GC (cfr. details in the supplementary data) was reproducible within a 2.1% relative standard deviation, corresponding to an expanded uncertainty of ± 3.4% expressed at the 95.5% confidence interval (CI) ($k = 3.31$ for a *t*-distribution with 3 degrees of freedom (4 stock solutions)).

The combined expanded uncertainty of gamma counting tissue activity measurements (U_{GC}) was always within ± 3.6% (expressed at the 95.5% CI), and was determined from the square root of the summation in quadrature of the uncertainty due to calibration reproducibility and the counting statistical error of the tissue sample.

2.7 Reference measurements for SPECT and GC activity calibrations

The reference activity concentrations of all ^{131}I stock solutions used for SPECT and GC activity calibrations were determined by high-resolution gamma spectrometry analysis using a high-purity germanium detector (model GC1818-7500SL; Mirion-Canberra, Meriden, USA) calibrated for photon energy and detection efficiency. More

details on the measurement procedure are provided in the supplementary data. The relative statistical uncertainty of the reference activity concentration of each of the calibration stock solutions was always within 1.6% at 95.5% CI (coverage factor $k = 2$).

2.8 Determination of SPECT activity recovery coefficients

Activity recovery coefficients (ARC) were calculated based on a SPECT study of a phantom filled with a [^{131}I]-NaI solution with a calibrated activity concentration of 10.4 MBq.mL^{-1}. The phantom is a 26-mm diameter cylindrical container made of acrylic plastic, with two fillable compartments containing various fillable rods. Both compartments (~ 4.4 mL) were filled, but only one compartment, containing two rods of 4- and 6-mm diameter and 32-mm length, was used for analysis. A 20-min SPECT scan of the whole phantom (120 bed positions, 10 seconds per position) was acquired. SPECT images were generated with the same image reconstruction and correction settings as for mouse scans. A cylindrical VOI was defined at the centre of each rod with a diameter equal to the diameter of the rod and a length of 4 mm. ARC were calculated, for each rod, as the ratio of the mean activity concentration of the VOI and the reference activity concentration of the ^{131}I solution at the start of the SPECT scan.

To assess the impact of lower counts on activity recovery, the phantom scan was reconstructed using only 10.0%, 5.0%, 2.5%, 1.0%, 0.5% and 0.1% of the counts from the list-mode data. These reconstructions emulate scans with lower activity concentrations equivalent respectively to 1.044, 0.522, 0.261, 0.104, 0.052 and 0.010 MBq.mL^{-1}.

Additional cylindrical VOIs, each with 4-mm height and 4-mm diameter, were drawn along the 4-mm rod. These VOIs were repeated on 6 planes (*i.e.* 7 VOIs in total) for an axial distance of 30 mm. For each activity concentration reconstructed, the statistical uncertainty of activity recovery (U_{Rec}) due to the regional (VOI) variability of the SPECT image counts within the rods was estimated, at the 95.5% CI, as:

$$U_{Rec} = \frac{k \cdot \sigma_{VOIs}}{\bar{A}_{VOIs} \cdot \sqrt{n_{VOIs}}} \qquad Eq.\ 3$$

Where σ_{VOIs} and $\bar{A}_{VOIs}$ are respectively the standard deviation and the mean of the VOI activities determined in all the VOIs (n_{VOIs}=7 VOIs); and k is the coverage factor, which is equal to 2.52 for a t-distribution with 6 (n_{VOIs}-1) degrees of freedom. This metric captures the statistical uncertainty in the activity recovery in the VOIs, and is used in this study as an indicator of the precision of the SPECT reconstruction to recover the activity in mouse kidneys with varying levels of activity concentration.

3 Results

3.1 SPECT activity recovery coefficients and the effect of activity concentration

The ARC determined from the phantom image with 10.4 MBq.mL^{-1} were 0.78 and 0.85 respectively for the 4- and 6-mm-diameter rods, indicating a partial (respectively 78% and 85%) recovery of the reference activity present within the rods.

The effect of lower activity concentrations (from reconstructing with fewer counts) in the local (voxel) and regional (VOI) activity recovery is shown respectively in Figs. 1 and 2. Inside the 6-mm rod (Fig. 1 (b)), an overshoot appears

somewhat near the rod edge, whereas an undershoot appears in the centre, which we tentatively attribute to the Gibbs effect. The overshoot-undershoot delta becomes more pronounced in the reconstructions of lower activity concentrations. For both rods, the variability of the locally reconstructed activity concentration within the rod increases with decreasing activity concentrations. At a regional level, the mean ARC decreases by just a few percent for the lowest concentrations, yet the statistical uncertainty in VOI activity recovery, U_{Rec}, significantly increases for concentrations below 0.1 MBq.mL^{-1}.

3.2 Mice studies

Representative examples of the SPECT and CT images and the VOIs used for quantification are shown in Fig. 3. At early time points (≤ 6 h), the predominant uptake in kidneys is clearly visualized on the SPECT images. At late time points (≥ 24 h), the SPECT images appear less uniform, the radioligand is more widespread in other abdominal tissues (e.g. liver, intestines) and kidney uptake is less evident.

3.2.1 Accuracy of SPECT-based activity quantification

Figure 4 illustrates the pharmacokinetic profile of the [^{131}I]-sdAb in the kidney, for the datasets used to evaluate the accuracy of SPECT-based kidney activity quantification (SS1 *vs* GC1). Figure 5 illustrates the mouse-specific pharmacokinetic profile of the [^{131}I]-sdAb for each of the *FIA/g* datasets acquired with longitudinal *in vivo* SPECT in a single mouse (LS1-LS5), as well as the pharmacokinetic profile of the GC dataset with additional time points (GC1ext).

The mean kidney *FIA/g* (of left and right kidneys of all mice per time point, ±SD) determined via GC were 0.26 ± 0.065, 0.057 ± 0.0056, 0.014 ± 0.0032, 0.0017 ± 0.0002, 0.0006 ± 0.0001 and 0.0005 ± < 0.0001 g^{-1}, respectively at approximately 1.5, 3.2, 6.6, 24, 48 and 73 h after the radioligand injection. The radioligand uptake in the kidneys is the highest at the earliest time point and decreases rapidly over time, with only about 5%, 0.6% and 0.2% of the activity measured at 1.5 h remaining in the kidney after respectively 6.6, 24 and 73 h p.i.

SPECT-based activities tend to underestimate the reference activity by an amount that is related to the ^{131}I activity concentration in the kidney, which is dependent on the time point of the pharmacokinetic profile of the [^{131}I]-sdAb (see Fig. 6). This underestimation is statistically significant for all time points (p-value < 0.01) and is on average − 12% at 1.5 h (2.78 MBq.mL^{-1} mean reference kidney activity concentration), -13% at 6.6 h (143 kBq.mL^{-1}), -40% at 24 h (15 kBq.mL^{-1}) and − 46% at 73 h (5 kBq.mL^{-1}) p.i.

3.2.2 Time-integrated pharmacokinetic parameter ã/M

The coefficients of the power function fits and the time-integrated activity coefficient per mass of tissue $\tilde{a}/M$ of all GC and SPECT measurement datasets are listed in Table 3. The R^2 values of the fit functions were 0.936, 0.925 and 0.929 respectively for datasets SS1, GC1 and GC1ext, indicating a strong correlation between the measured *FIA/g* values and the values estimated by the power function fit for the three datasets, derived from multiple sacrificed mice. The R^2 values of the fit functions of the LS datasets were all > 0.999, indicating an even stronger correlation between measured and curve fit-estimated *FIA/g* data.

Concerning the comparison of SPECT against GC (Table 3). The $\tilde{a}/M$ value of SPECT dataset SS1 was − 15% lower than that of GC dataset GC1 determined on the same mice. Similar or larger deviations from the reference

$\tilde{a}/M$ value of dataset GC1ext are observed with longitudinal SPECT datasets (*in vivo* scans), ranging from − 13% to -26% (-19% mean deviation of 5 mice), depending on the mouse investigated (Table 3).

Aiming to compensate to some extent for partial recovery of SPECT images in the pharmacokinetic assessment, a partial recovery correction (PRC) factor equal to the inverse of the ARC of the 6-mm rod (*i.e.* PRC factor equal to 1.176) was applied to all kidney activities determined with SPECT. New curve fits were determined and $\tilde{a}/M$ was estimated for the SS1 and LS datasets. The PRC increases the $\tilde{a}/M$ values by a factor equal to the PRC factor, which reduces the range of deviation from the reference values (GC1ext) to just 2% for dataset SS1 and to less than ± 15% for all the LS datasets (Table 3).

Table 3. Overview of power function fit coefficients (c_1 and c_2) and time-integrated activity coefficient per mass of tissue ($\tilde{a}/M$) obtained from various datasets of the left kidney *FIA/g* determined with GC or SPECT; and the effect of applying a partial recovery correction (PRC) to SPECT activities.-

Dataset [technique]	**No of mice, *n***	**No of time points**	Without PRC				With PRC = 1/0.85	
			Function coefficients		**$\tilde{a}/M$ (h.g^{-1})**	**% dev. from GC1ext $\tilde{a}/M$**	**$\tilde{a}/M$ (h.g^{-1})**	**% dev. from GC1ext $\tilde{a}/M$**
			c_1 (g^{-1})	**c_2**				
GC1 [GC]	14	4	0.547	1.90	0.409	2%	-	-
SS1 [SPECT]	14	4	0.481	1.92	0.348	-14%	0.409	2%
GC1ext [GC]	20	6	0.551	1.92	0.402	-	-	-
LS1 [SPECT]	1	6	0.314	1.65	0.339	-16%	0.399	-1%
LS2 [SPECT]	1	6	0.326	1.66	0.351	-13%	0.413	3%
LS3 [SPECT]	1	6	0.348	1.77	0.312	-22%	0.367	-9%
LS4 [SPECT]	1	6	0.314	1.74	0.297	-26%	0.350	-13%
LS5 [SPECT]	1	6	0.428	1.88	0.330	-18%	0.389	-3%

4 Discussion

The kidneys are often on of the main organs of interest in biodistribution and dose-effect radiobiological investigations in basic and (preclinical) (back)translational radiopharmaceutical research. An accurate quantification of radionuclide activity in mouse kidney tissues *in vivo* using quantitative micro-SPECT imaging would be useful to derive accurate pharmacokinetic data and enable accurate dose estimations required to support such studies. Therefore, this study investigated the accuracy of activity quantification in mouse kidneys using a commercial micro-SPECT/CT system, for the mouse biodistribution conditions of a radioligand with significant kidney uptake.

In this study *ex vivo* gamma counting was used as the reference method for determining the reference ^{131}I activity in mouse kidneys because of its high measurement sensitivity and quantitative accuracy and its widespread use in preclinical research. The measurement protocol was optimized to limit (or control) some systematic (activity calibration, linearity, cross-talk, volume effects) and statistical (measurement counts) uncertainty of GC measurements to increase the confidence in the reference values.

Activity measurements with GC and SPECT were both directly traceable to high-resolution gamma spectrometry, to limit the influence of errors associated to the reproducibility and accuracy of the activity calibration procedures of the two techniques in the evaluation of SPECT accuracy.

4.1 Accuracy of SPECT-based kidney activity quantification

Several factors affect the quantitative accuracy of SPECT, including (i) non-uniform photon attenuation and (ii) scatter [4]; (iii) partial volume effects [4]; (iv) statistical and bias effects associated to the image reconstruction methods in relation with some imaging conditions [6]; (v) activity calibration procedure; etc. Moreover, quantification of radioactivity in tissues based on *in vivo* SPECT studies can be affected also by (vi) the methods used for image analysis, and (vii) the variation of the radioligand biodistribution over time relative to the imaging scan duration.

In this study, photon attenuation (i) was compensated based on the attenuation map derived from CT data acquired on the same mouse used for SPECT imaging [10]. (Compton) photon scatter (ii) was compensated via the triple-energy-window method [9]. Both compensations were implemented using the vendor-provided software of the imaging system. A verification of the accuracy of these compensations was beyond the scope of this study.

SPECT images were reconstructed with the vendor-provided software of the imaging system using pixel-based OSEM with resolution recovery and compensation for distance-dependent pinhole sensitivity and a dedicated system matrix for (^{131}I) 364 keV photons [18, 19].

4.1.1 Phantom study

To correct for the combined effect of partial volume (iii) and reconstruction (iv) effects a SPECT phantom study was performed to quantify the SPECT activity recovery coefficient, for specific imaging and reconstruction settings.

Significant PVE are expected for the imaging tasks investigated because of the rather large pinhole diameter (1.6 mm) of the SPECT collimator used, which enhances photon detection sensitivity at the expense of degrading the system spatial resolution [4, 2]. Additionally, imaging of ^{131}I can be challenging because of the higher energy of the photons used for imaging (365 keV) and the presence of significant photon emissions of even higher energies (around 9% yield of 637 and 722 keV gammas), which increases pinhole edge and collimator penetration effects, both of which have a degrading effect on spatial resolution and therefore on PVE [2].

Generally, for the phantom setting, PVE lead to an underestimation of the activity quantified with rod-delimited VOIs. As expected, the influence of PVE is larger for smaller objects, therefore the ARC is lower for the 4-mm rod (0.78) compared with the 6-mm rod (0.85).

Iterative reconstruction methods, including OSEM algorithms, are the current method of choice for quantitative image reconstruction in SPECT. Both Gibbs and noise artefacts are however known effects of these methods [7]. Gibbs artefacts have been associated to the use of resolution modelling—a kind of compensation indeed implemented in the algorithm used in this study for image reconstruction; and can lead to a positive bias (overestimation), or under certain circumstances a negative bias (underestimation), in activity quantification [21, 22].

For the imaging settings of the phantom scan, the reconstruction of lower activity concentrations (i.e. lower scan counts) impacts mostly the precision (U_{Rec}) rather than the bias (mean ARC) of activity quantification with the regional VOI. Low-counts reconstructions are more prone to noise, which can increase the statistical uncertainty in activity quantification in the VOI, as indicated by the larger U_{Rec} values found with the lowest simulated activity concentrations. The somewhat lower mean ARC values observed with decreasing concentration of counts might be due to an additional negative bias from the reconstruction, and/or due to the need of more iterations, since the image reconstruction of regions with lower counts are known to converge more slowly than high-count regions [23].

To note, the count fractionation used to simulate lower activity (or shorter) scans does not discriminate between counts associated to ^{131}I radiations and true background counts, which are independent on the activity scanned and whose count rate should remain constant over any acquisition time. Thus, compared with an image that was actually acquired with a low activity (or a short acquisition time), a simulated low-count image will have a fixed signal-to-background ratio and will be less affected by the background fluctuations. This means that for actual low activity-concentration studies the decrease in the mean ARC and the increase in U_{Rec} might possibly be larger (i.e. worse) than predicted here from simulated images (Fig. 5).

4.1.2 Mice studies

With the imaging and quantification settings used in this study, micro-SPECT tends to underestimate the ^{131}I activity of [^{131}I]-sdAb present in mouse kidneys. The amount of underestimation is considerably larger for the late time points of the pharmacokinetic profile of the [^{131}I]-sdAb (≥ 24 h p.i.), when the kidney activity concentrations are below 25 kBq.mL^{-1}.

To limit the reproducibility uncertainty in SPECT quantification due to an arbitrary selection of VOI size, a consistent approach for activity quantification was used in which for each mouse kidney the size of the VOI was adjusted to match the estimated volume of the kidney. Ellipsoidal VOIs were used, generally resembling well the shape of mouse kidneys, while providing a convenient and reproducible solution for VOI delineation of SPECT images in which the activity distribution is not always uniform within kidney tissues, and/or the SPECT (or CT) image contrast and/or quality are not optimal to define accurate isocontour-based VOIs of the kidneys. Although an ellipsoidal VOI does not provide an optimal fit of the shape of just any mouse kidney, the error (variability) in activity quantification resulting from this approach is expected to be smaller than the error from using a subjective VOI size.

Concerning the combined effects of partial volume (iii) and image reconstruction (iv), the mean radii of the kidney ellipsoidal VOIs of all the mice imaged with SPECT were 2.4, 2.9 and 5.1 mm. Thus, for a PVE analysis one may approximate a mouse kidney roughly as a rod with a radius of 3 mm. The ARC of a kidney when the activity

concentration in adjacent tissues is negligible would then be around 0.85, which could explain the A_{SPECT}/A_{GC} values obtained at 1.5 and 6.6 h and to some extent at 24 and 73 h p.i. (Fig. 6).

The lower A_{SPECT}/A_{GC} values obtained at 24 and 73 h indicate the presence of an additional source of negative bias in the reconstructed kidney activities of scans taken at late time points. We hypothesize that this bias is related to the (larger) impact of low-counts image reconstruction effects in these images with much lower ^{131}I activity concentration present in kidney tissues. Overall, the pharmacokinetics of the [^{131}I]-sdAb in mouse healthy tissues are fast, with less than 3% of the injected activity remaining in the mouse body after 24 h of administration. Compared to scans taken at 1.5 h p.i., the approximately 160- and 550-times lower kidney activity concentrations imaged at respectively 24 and 73 h far outweigh the about 3.5-times longer acquisition durations used for the late scans. The counts potentially useful for imaging the uptake of [^{131}I]-sdAb in the kidneys would still be in the order of 50- and 150-times lower for the late scans compared to the earliest scan. Moreover, the background-and-scatter to photo-peak counts fraction was significantly larger for the late scans (around 44% and 51% respectively at 24 and 73 h) compared to the earlier scans (11% and 22% respectively at 1.5 and 6.6 h), which renders the reconstructions of the late scans more prone to the effects of noise. Thus, considering the much lower number of “useful” counts expected to be available for reconstruction and the expected increased noise effects of the late scans, and based on the analysis of the rod mean ARC and the U_{Rec} of reconstructions with lower counts of the phantom scan, we expect the kidney activity recovery of image reconstructions from the late scans to be affected by a larger negative bias and larger statistical uncertainty compared with earlier (1.5 and 6.6 h) scans. This reasoning might explain, at least partly, the larger underestimations of the reference kidney activities obtained at 24 and 73 h p.i.

Finally, regarding the influence of the variation of kidney uptake over (scan) time in the evaluation of accuracy of SPECT activities, the kidney activities at the moment of the late scans would still be very low despite the 2%-to-5%-higher uptake expected at the middle time of the *in vivo* scans (compared with the uptake at time of death), so the potential over-response in SPECT-based activities expected from this effect is outweighed by the effects associated to low-counts studies mentioned above.

4.2 Time-integrated pharmacokinetic parameter $\tilde{a}/M$ and longitudinal *in vivo* SPECT studies

For a fixed mathematical model, the accuracy of the estimation of the time-integrated $\tilde{a}/M$ coefficient depends on the accuracy of the time-*FIA/g* data, as well as the goodness of fit of the mathematical model to the data. Curve fits of SPECT dataset SS1 and GC datasets GC1 and GC1ext had similar R^2 values, thus differences in the $\tilde{a}/M$ values estimated from different datasets are most likely due to differences in the kidney activity values measured with the two techniques.

Because of the much larger amount of activity present in the kidneys at early time points and the fast pharmacokinetics of the [^{131}I]-sdAb, the $\tilde{a}/M$ estimation is influenced mostly by the activity measured at the early time points. Despite the large (≥ 28%) underestimations associated with A_{SPECT} values of late time points, the $\tilde{a}/M$ value is only around 15% lower with SPECT compared with GC and as such follows approximately the level of underestimation of A_{SPECT} of early time points (~ 12%). This is also the reason why a correction for partial activity recovery (PRC) of just 1/0.85 for all A_{SPECT} values was sufficient to reduce the difference between the $\tilde{a}/M$ values estimated with GC and SPECT SS1 to just 2% (cfr. Table 3).

This study demonstrates the feasibility of deriving quantitative mouse-specific kidney pharmacokinetic data from longitudinal *in vivo* SPECT studies of kidney ^{131}I activity quantification. Compared with the pharmacokinetic datasets derived from multiple mice (GC1, GC1ext, SS1), the R^2 values of the fit functions were especially good (> 0.999) for the datasets derived with *in vivo* SPECT, which might result from the fact that in a longitudinal SPECT study each mouse acts as its own control for time-point sampling, therefore eliminating the impact of mouse inter-variability in the pharmacokinetics assessment. This can be an important gain of SPECT over conventional GC methods when a more accurate investigation of the time dependence of pharmacokinetics is of interest, such as for tissue dosimetry for targeted radionuclide therapy. The variation in the $\tilde{a}/M$ values of different mice (LS1-LS5) and in their deviations from the reference $\tilde{a}/M$ value (dataset GC1ext) might just reflect mouse inter-variability, or a combination of the latter with an error in SPECT activity quantification due to a non-negligible change in kidney uptake during the rather long SPECT acquisition especially at early time-points (1.0 and 3.3 h p.i.) with fast pharmacokinetics of the [^{131}I]-sdAb in the kidneys. Shorter scan acquisitions (e.g. of few minutes) are feasible and can be used to reduce that source of uncertainty.

5 Conclusion

The quantitative accuracy of radioactivity quantification in mouse tissues using micro-SPECT can be affected by partial recovery of the imaged activity and variability in the reconstructed SPECT image. For the micro-SPECT imaging system and the quantification methodology used, this leads to a significant underestimation in the amount of ^{131}I activity in mouse kidneys quantified with SPECT.

Nevertheless, the SPECT imaging system used, combined with a robust activity quantification methodology, allows to derive reasonably accurate (within − 15% from GC) time-integrated pharmacokinetic information of the ^{131}I-labelled sdAb investigated in mouse kidneys. This outcome is satisfactory, considering the benefits associated with non-toxic *in vivo* methods vis-à-vis analogues *ex vivo* methods. For example, mouse-specific absorbed dose estimates enabled by *in vivo* quantitative SPECT might offer a gain in efficacy in finding and establishing sound preclinical absorbed dose-effect relationships in targeted radionuclide therapy, in view of the potential mouse inter-variability effects implicit in dose-effect studies in which tissue dosimetry is based on pharmacokinetic information derived (*ex vivo*) from mice groups different from those utilized for evaluating biological response. Also, since *in vivo* SPECT obviates the need of multiple experimental groups for time sampling to assess the pharmacokinetic profile, it may allow a reduction in the overall animal burden of preclinical pharmacokinetic and biological effect investigations, which implies an important gain from an animal ethics perspective as laid out by the 3R principle (Replacement, Reduction, Refinement) [24]. Last but not least, better quantitative accuracy in SPECT-based time-integrated pharmacokinetic data is achievable by applying an appropriate correction for partial recovery to the SPECT-quantified kidney activities. In this study, a PRC based on the ARC determined in a phantom setting allowed to reduce the deviation between the $\tilde{a}/M$ values of SPECT and GC to just 2%. This gain in quantitative accuracy can be particularly meaningful, for instance, in investigations in which an accurate evaluation of the dose-effect relationship is required, e.g. to allow a sound comparison of the dose-related nephrotoxicity risk of different radioligand therapies. Overall, these gains continue to bring forward the use of micro-SPECT imaging for preclinical quantitative imaging studies of drug pharmacokinetics in basic and (back)translational research.

Abbreviations

[^{131}I]SGMIB
N-Succinimidyl 4-guanodinomethyl-3-[^{131}I]iodobenzoate
ARC
activity recovery coefficient
CI
confidence interval
CT
computed tomography
GC
gamma counting
OSEM
ordered subset expectation maximization
p.i.
post injection
PRC
partial recovery correction
PVE
partial volume effects
SD
standard deviation
sdAb
single-domain antibody fragment
SPECT
single-photon emission computed tomography
VOI
volume of interest

Declarations

Ethics approval and consent to participate

All animal experiments were conducted in accordance with the guidelines and after approval of the Ethical Committee of the Vrije Universiteit Brussel.

Consent for publication

Not applicable.

Availability of data and material

The data that support the findings of this study are available from the corresponding author upon reasonable request.

Competing interests

MD is co-founder and employee of Precirix SA and holds ownership interest (including patents) in sdAb diagnostics and therapeutics. The other authors declare that they have no competing interests.

Funding

This study was funded by the Belgian Nuclear Research Centre and the Vrije Universiteit Brussel. MD is a postdoctoral researcher of the Research Foundation Flanders - FWO (12H3619N).

Authors' contributions

CSV, LS, PC, MD and VC contributed to the conception and design of the study. CSV and PC acquired (part of) the measurement data. CSV analysed the data and drafted the manuscript. All authors critically revised the manuscript.

Acknowledgements

The authors kindly thank Cindy Peleman (VUB) for technically assisting in the animal experiments, Jos Eersels (VUB) for radiolabelling the sdAb and Prof. Dr. Michel Defrise for his scientific advice regarding the SPECT studies and the manuscript.

Authors' information

[1]Radiation Protection Dosimetry and Calibrations, Belgian Nuclear Research Centre (SCK CEN), Mol, Belgium. [2]Department of Medical Imaging, Laboratory for In Vivo Cellular and Molecular Imaging, Vrije Universiteit Brussel, Brussels, Belgium.

References

1. Bernsen MR, Vaissier PEB, Van Holen R, et al. The role of preclinical SPECT in oncological and neurological research in combination with either CT or MRI. Eur J Nucl Med Mol Imaging. 2014;41(Suppl 1):36–49. doi:10.1007/s00259-013-2685-3.
2. Meikle SR, Kench P, Kassiou M, Banati RB. Small animal SPECT and its place in the matrix of molecular imaging technologies. Phys Med Biol. 2005;50(22):R45–61. doi:10.1088/0031-9155/50/22/R01.
3. Deleye S, Van Holen R, Verhaeghe J, et al. Performance evaluation of small-animal multipinhole μSPECT scanners for mouse imaging. Eur J Nucl Med Mol Imaging. 2013;40(5):744–58. doi:10.1007/s00259-012-2326-2.
4. Hwang AB, Franc BL, Gullberg GT, Hasegawa BH. Assessment of the sources of error affecting the quantitative accuracy of SPECT imaging in small animals. Phys Med Biol. 2008;53(9):2233–52. doi:10.1088/0031-9155/53/9/002.

5. Finucane CM, Murray I, Sosabowski JK, et al. Quantitative Accuracy of Low-Count SPECT Imaging in Phantom and In Vivo Mouse Studies. Int J Mol Imaging. 2011;2011:197381. doi:10.1155/2011/197381.
6. Qi J, Leahy RM. Iterative reconstruction techniques in emission computed tomography. Phys Med Biol. 2006;51:R541–78. doi:10.1088/0031-9155/51/15/R01.
7. Snyder DL, Miller MI, Thomas LJ, Politte DG. Noise and Edge Artifacts in Maximum-Likelihood Reconstructions for Emission Tomography. IEEE Trans Med Imaging. 1987;6(3):228–38. doi:10.1109/TMI.1987.4307831.
8. Frey EC, Humm JL, Ljungberg M. Accuracy and Precision of Radioactivity Quantification in Nuclear Medicine Images. Semin Nucl Med. 2012;42(3):208–18. doi:10.1053/j.semnuclmed.2011.11.003.
9. Ogawa K, Harata Y, Ichihara T, Kubo A, Hashimoto S. A practical method for position-dependent Compton-scatter correction in single photon emission CT. IEEE Trans Med Imaging. 1991;10:408–12.
10. Wu C, de Jong JR, Gratama van Andel HA, et al. Quantitative multi-pinhole small-animal SPECT: uniform versus non-uniform Chang attenuation correction. Phys Med Biol. 2011;56:N183–93.
11. Ljungberg M, Gleisner KS. 3-D Image-Based Dosimetry in Radionuclide Therapy. IEEE Trans Radiat Plasma Med Sci. 2018;2(6):527–40.
12. Vanhove C, Bankstahl JP, Krämer SD, et al. Accurate molecular imaging of small animals taking into account animal models, handling, anaesthesia, quality control and imaging system performance. EJNMMI Phys. 2015;2(1):31. doi:10.1186/s40658-015-0135-y.
13. Denis-Bacelar AM, Cronin SE, Da Pieve C, et al. Pre-clinical quantitative imaging and mouse-specific dosimetry for 111In-labelled radiotracers. EJNMMI Res. 2016;6(1):85. doi:10.1186/s13550-016-0238-z.
14. D'Huyvetter M, De Vos J, Xavier C, Pruszynski M, Sterckx YGJ, Massa S, et al. ^{131}I-labeled Anti-HER2 Camelid sdAb as a Theranostic Tool in Cancer Treatment. Clin Cancer Res. 2017;23(21):6616–28. doi:10.1158/1078-0432.CCR-17-0310.
15. D'Huyvetter M, De Vos J, Caveliers V, et al. Phase I trial of ^{131}I-GMIB-Anti-HER2-VHH1, a new promising candidate for HER2-targeted radionuclide therapy in breast cancer patients. J Nucl Med. 2020. doi:https://doi.org/10.2967/jnumed.120.255679.
16. Vaneycken I, Devoogdt N, Van Gassen N, Vincke C, Xavier C, Wernery U, et al. Preclinical screening of anti-HER2 nanobodies for molecular imaging of breast cancer. FASEB J. 2011;25:2433–46. doi:10.1096/fj.10-180331.
17. Goorden MC, van der Have F, Kreuger R, et al. VECTor: a preclinical imaging system for simultaneous submillimeter SPECT and PET. J Nucl Med. 2013;54:306–12.
18. Branderhorst W, Vastenhouw B, Beekman FJ. Pixel-based subsets for rapid multi-pinhole SPECT reconstruction. Phys Med Biol. 2010;55:2023–34.
19. van der Have F, Ivashchenko O, Goorden MC, et al. High-resolution clustered pinhole ^{131}Iodine SPECT imaging in mice. Nucl Med Biol. 2016;43(8):506–11. doi:10.1016/j.nucmedbio.2016.05.015.
20. Loening AM, Gambhir SS. AMIDE: A Free Software Tool for Multimodality Medical Image Analysis. Molecular Imaging. 2003;2(3):131–7. doi:10.1162/153535003322556877.
21. Thielemans K, Asma E, Ahn S, et al. Impact of PSF modelling on the convergence rate and edge behaviour of EM images in PET. IEEE Nuclear Science Symposium Conference & Medical Imaging Conference Record, 2010;:3267–3272. doi:10.1109/NSSMIC.2010.5874409.

22. Seret A, Nguyen D, Bernard C. Quantitative capabilities of four state-of-the-art SPECT-CT cameras. EJNMMI Research. 2012;2(1):45. doi:10.1186/2191-219X-2-45.
23. Pan TS, Luo DS, Kohli V, King MA. Influence of OSEM, elliptical orbits and background activity on SPECT 3D resolution recovery. Phys Med Biol. 1997;42(12):2517–29. doi:10.1088/0031-9155/42/12/015.
24. Workman P, Aboagye EO, Balkwill F, et al. Guidelines for the welfare and use of animals in cancer research. Br J Cancer. 2010;102:1555–77.

Figures

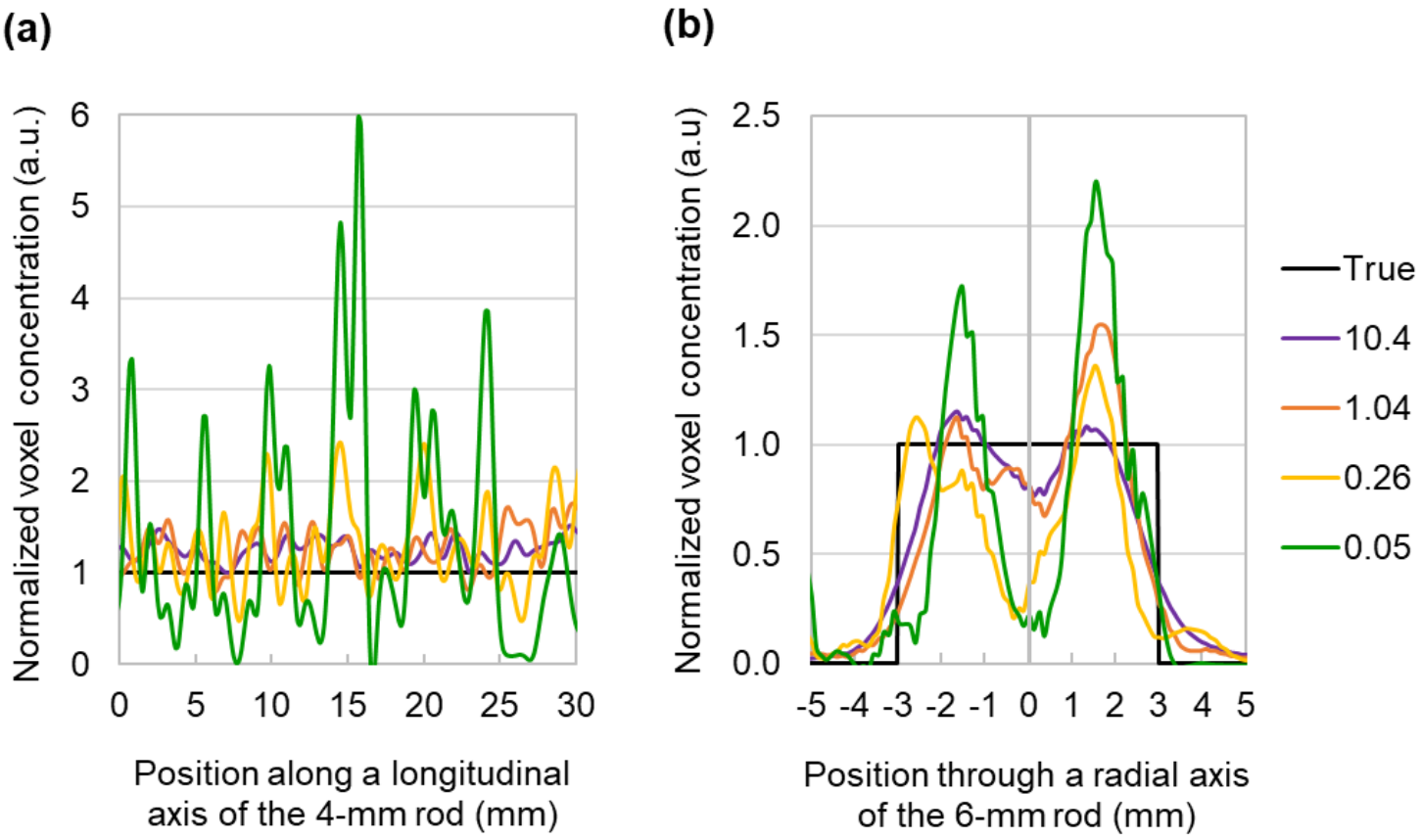

Figure 1

Longitudinal and radial profiles through respectively the 4-mm (a) and the 6-mm (b) rods, for various (simulated) 131I activity concentrations (series legend in MBq.mL-1) of the phantom scan.

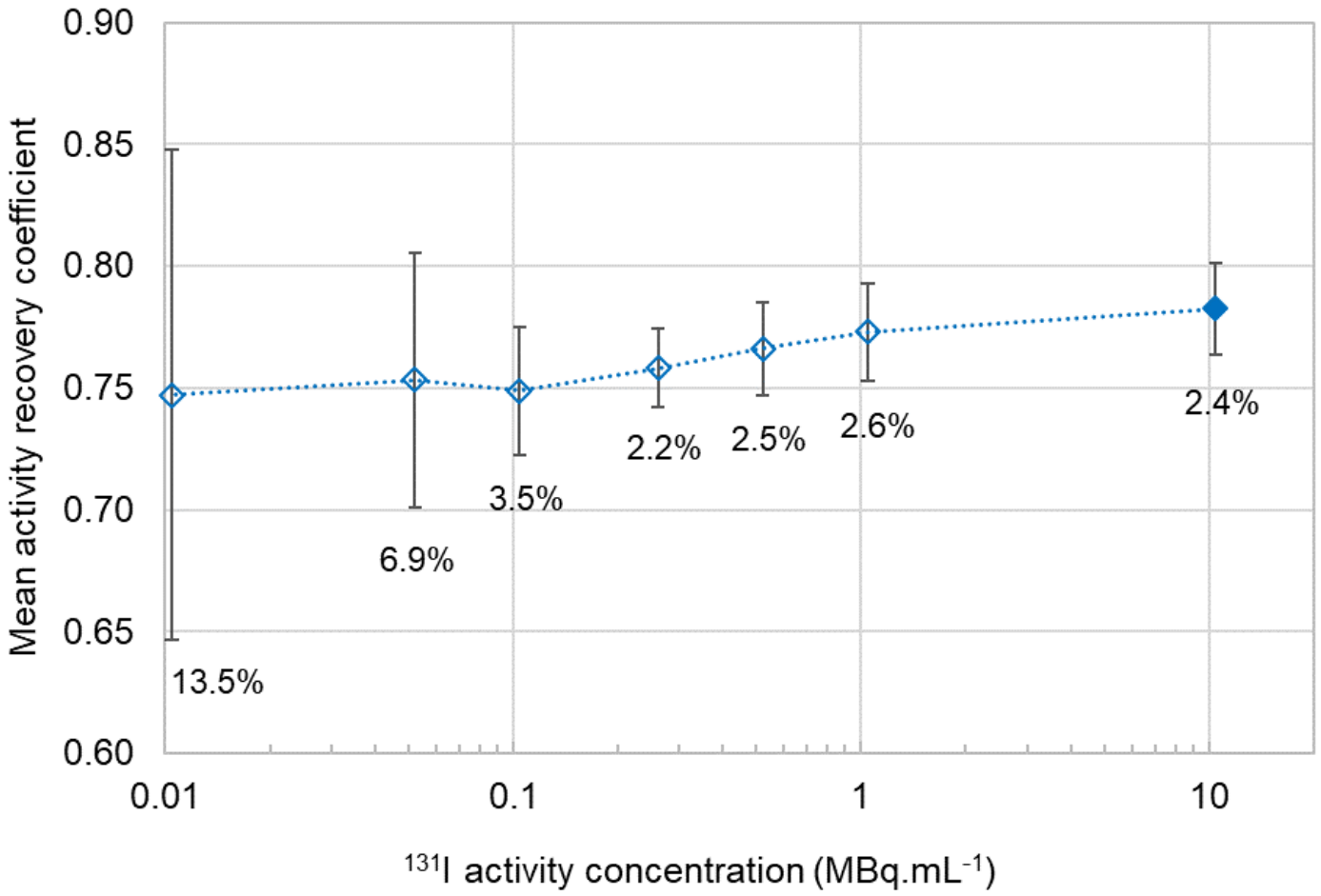

Figure 2

Mean ARC for the 4-mm rod for various 131I activity concentrations of the phantom scan. Empty symbols indicate ARC values obtained from reconstructions simulating activity concentrations lower than the activity concentration actually imaged (10.4 MBq.mL-1, ARC value indicated by the filled symbol). Error bars and labels indicate ± the expanded statistical uncertainty of activity recovery, URec, at the 95.5% CI.

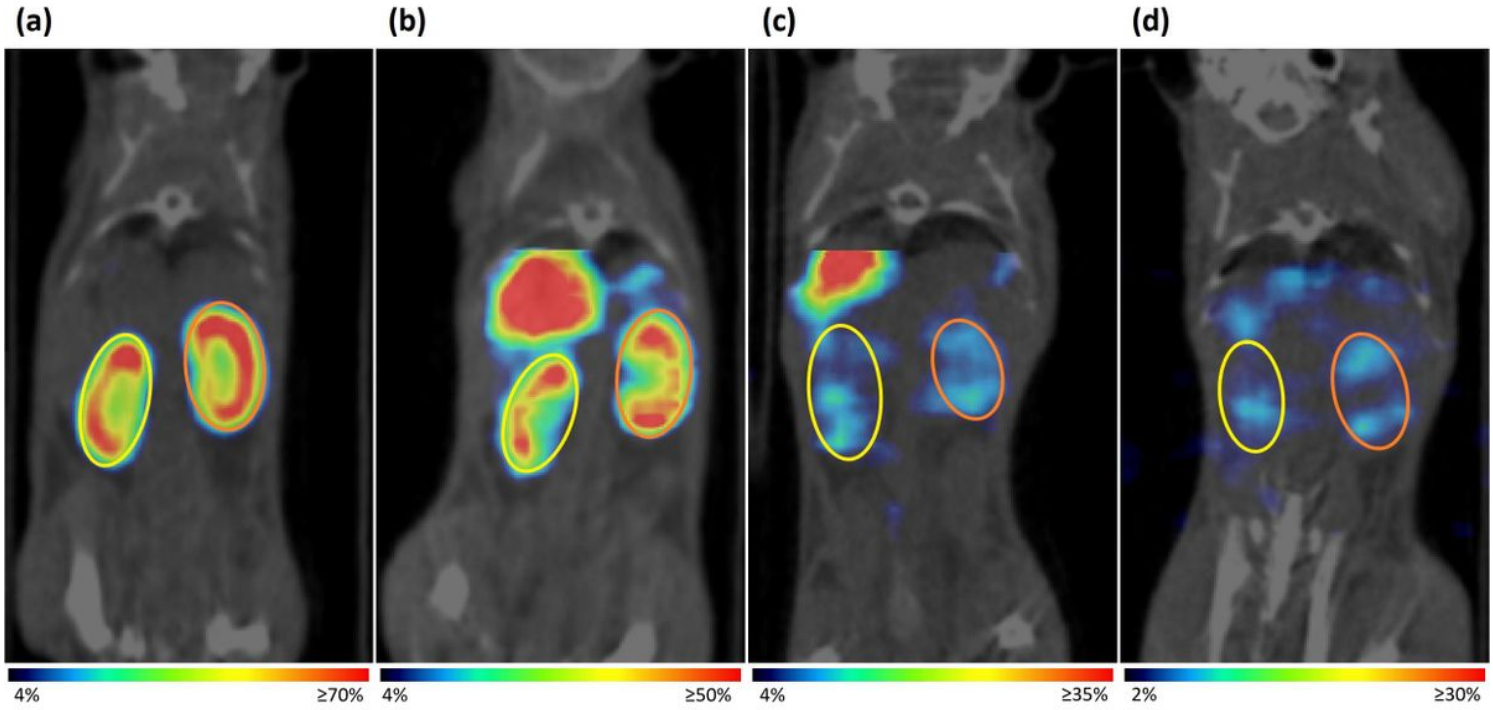

Figure 3

Overlays of SPECT and CT section images through the kidneys, sequentially acquired in vivo on the mouse of dataset LS5, at around 1 (a), 6 (b), 26 (c) and 73 (d) h p.i. of the [131I]-sdAb. VOIs used for activity quantification are shown in each sub-figure as an overlay in yellow (left kidney) and orange (right kidney) colours. High uptake above left kidney of sub-figures (b) and (c) corresponds to liver tissue.

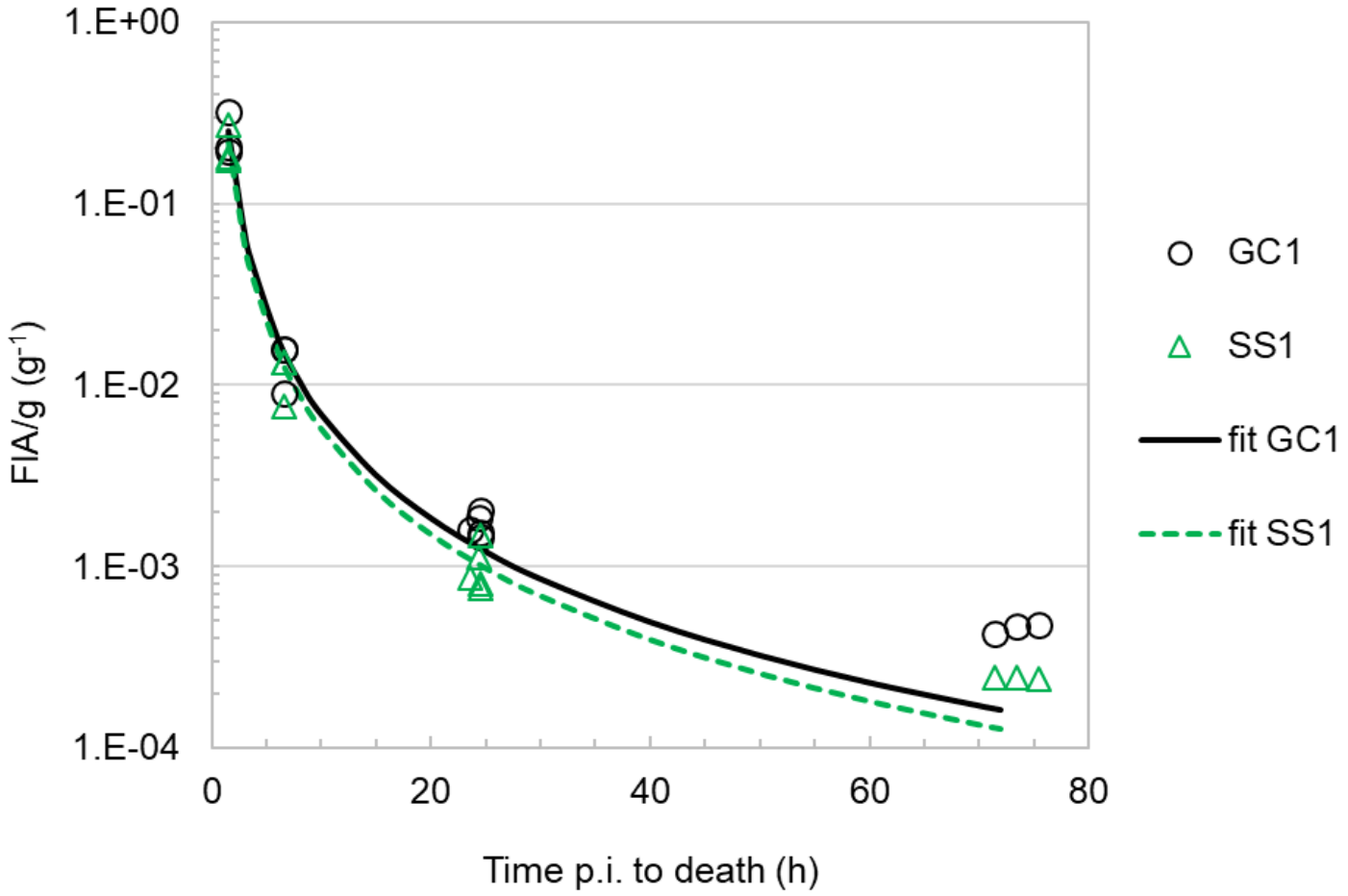

Figure 4

Time-FIA/g data of the left kidney determined with SPECT (dataset SS1) and with GC (dataset GC1), of 14 mice injected with the [131I]-labelled sdAb. The curves indicate the power function fit of each dataset (cfr. function coefficients in Table 3).

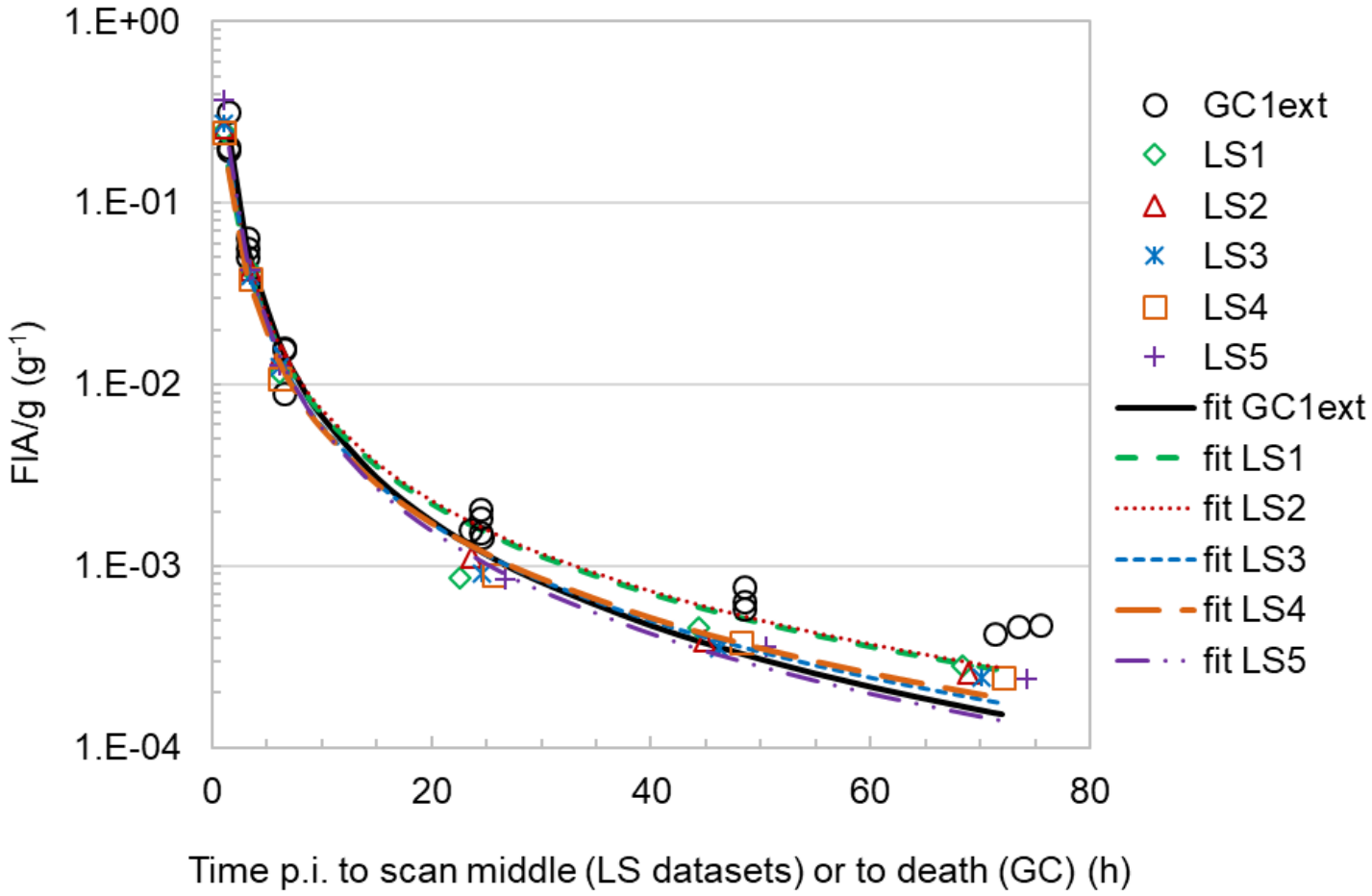

Figure 5

Time-FIA/g data of the left kidney determined with longitudinal in vivo SPECT imaging (datasets LS1-LS5) and with GC (dataset GC1ext), of respectively 5 (SPECT) and 20 (GC) mice injected with the [131I]-labelled sdAb. The curves indicate the power function fit of each dataset (cfr. function coefficients in Table 3).

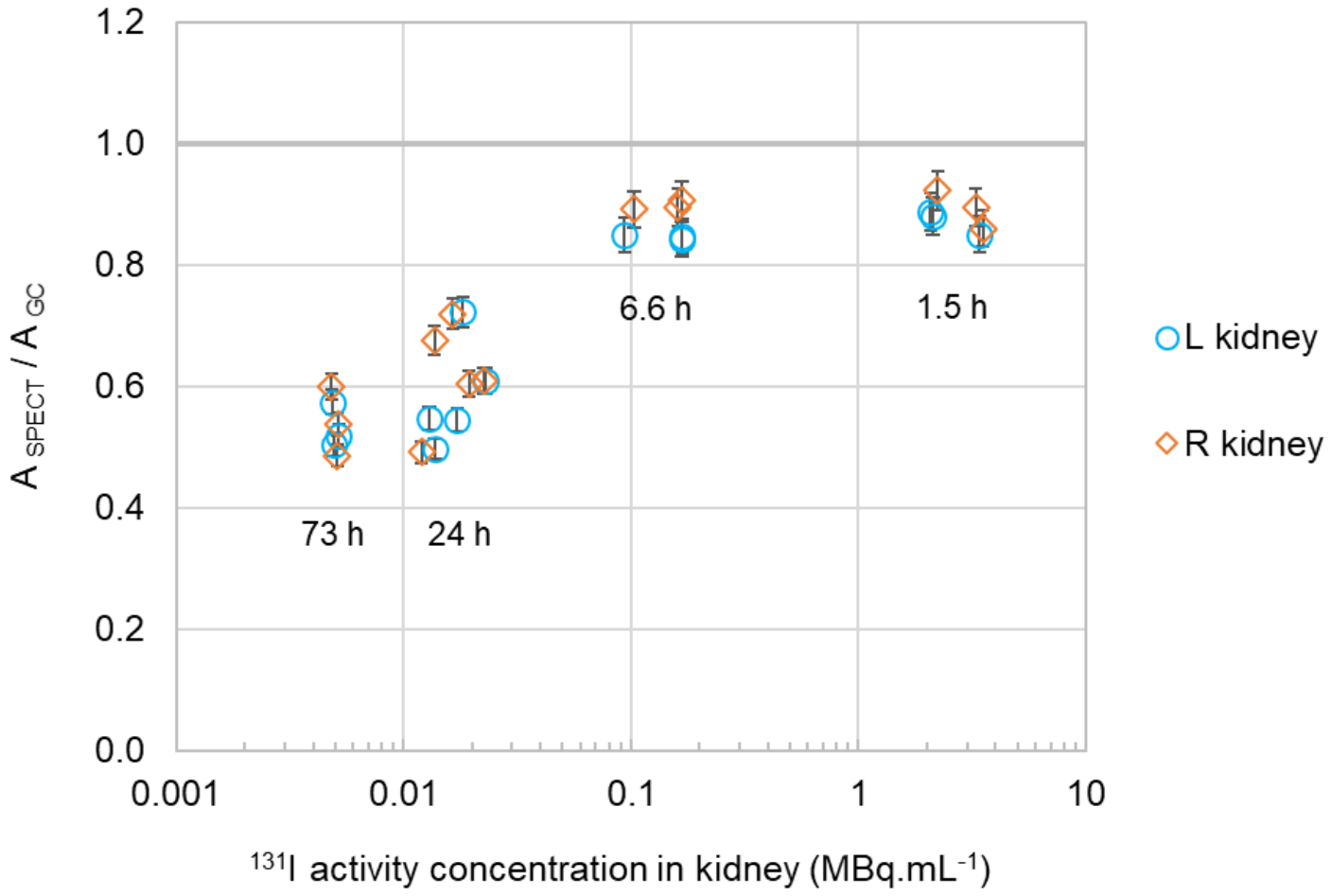

Figure 6

Ratios between the 131I activity in the kidney determined with SPECT (ASPECT) and the reference activity determined with GC (AGC) as a function of the reference activity concentration in the kidney, for all mice (n=14) of datasets GC1 and SS1. Each data symbol corresponds to one kidney of one mouse. Labels indicate the approximate time point of the pharmacokinetic profile to which a group of data symbols belong. Error bars indicate ± the expanded combined uncertainty of only GC measurements, UGC, at the 95.5% CI.

Supplementary Files

This is a list of supplementary files associated with this preprint. Click to download.

- 20210625supplementarydata.docx